Electronic Supplementary Material (ESI) for Nanoscale.
This journal is © The Royal Society of Chemistry 2019

Supporting Information

Interlayer engineering of $Ti_3C_2T_x$ MXene towards high capacitance supercapacitors

Minmin Hu, Renfei Cheng, Zhenjiang Li, Tao Hu, Hui Zhang, Chao Shi, Jinxing Yang, Cong Cui, Chao Zhang, Hailong Wang, Bingbing Fan, Xiaohui Wang and Quan-Hong Yang**

Experimental Section

Materials: Ti powder (99%, –300 mesh) was provided by Haixin (China), Al powder (99%, D50 = 10 μm) was obtained from AIFA (China), and C (99%, D90 = 6.5 μm) was purchased from TIMCAL (Switzerland). NH_3 (99.999%) was provided by Dalian Special Gases Co., LTD. Hydrofluoric acid (HF, 40%), hydrochloric acid (HCl, 36% – 38%), lithium fluoride (LiF, CP), calcium chloride ($CaCl_2$, AR), potassium hydroxide (KOH, AR), and N–methyl–2–pyrrolidinone (NMP, 99.8%) were purchased from Sinopharm Chemical Reagent Co., LTD. Polyvinylidene fluoride (PVDF) was obtained from Alfa Aesar. All the chemicals were used as received without further purification.

Computation methods: The density functional theory computations were performed using the Cambridge Sequential Total Energy Package. The electron-ion interaction was discribed by using plane-wave pseudopotential. The exchange correlation energy is described by the functional of GGA–PW91. The long-range interaction was considered by dispersion correction within the OBS and Grimme methods. The cutoff energy was set at 380 eV. To investigate the effect of N doping, supercells of $Ti_3C_2O_2$ with carbon vacancy and $Ti_3C_2O_2$ with carbon vacancy occupied by N were built, respectively. The Brillouin zone was represented by Monkhorst–Pack special k-point mesh of 5 × 5 × 1 for both geometry optimizations. For electronic structure computations, a larger k-point mesh of 9 × 9 × 1 was used. All atoms were allowed to move until the energy was less than 10^{-5} eV per atom and the force on each atom was less than 0.05 eV $Å^{-1}$.

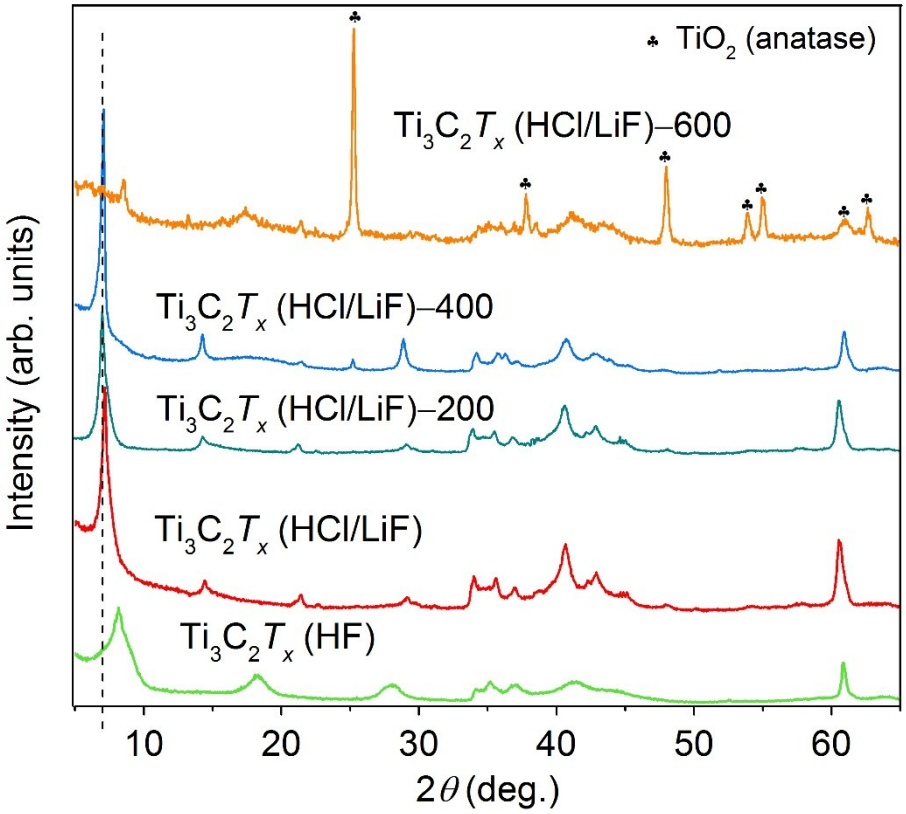

Fig. S1 XRD patterns of $Ti_3C_2T_x$ MXenes under various treatments. $Ti_3C_2T_x$–HF and $Ti_3C_2T_x$–(HCl/LiF) were produced via etching the MAX phase in HF and HCl–LiF solutions, respectively. $Ti_3C_2T_x$–(HCl/LiF)–200, $Ti_3C_2T_x$–(HCl/LiF)–400 and $Ti_3C_2T_x$–(HCl/LiF)–600 was obtained by heating $Ti_3C_2T_x$–(HCl/LiF) in ammonia atmosphere at 200, 400 and 600 °C. For $Ti_3C_2T_x$–(HCl/LiF)–600, TiO_2 was observed due to the oxidation of $Ti_3C_2T_x$ at too high temperature.

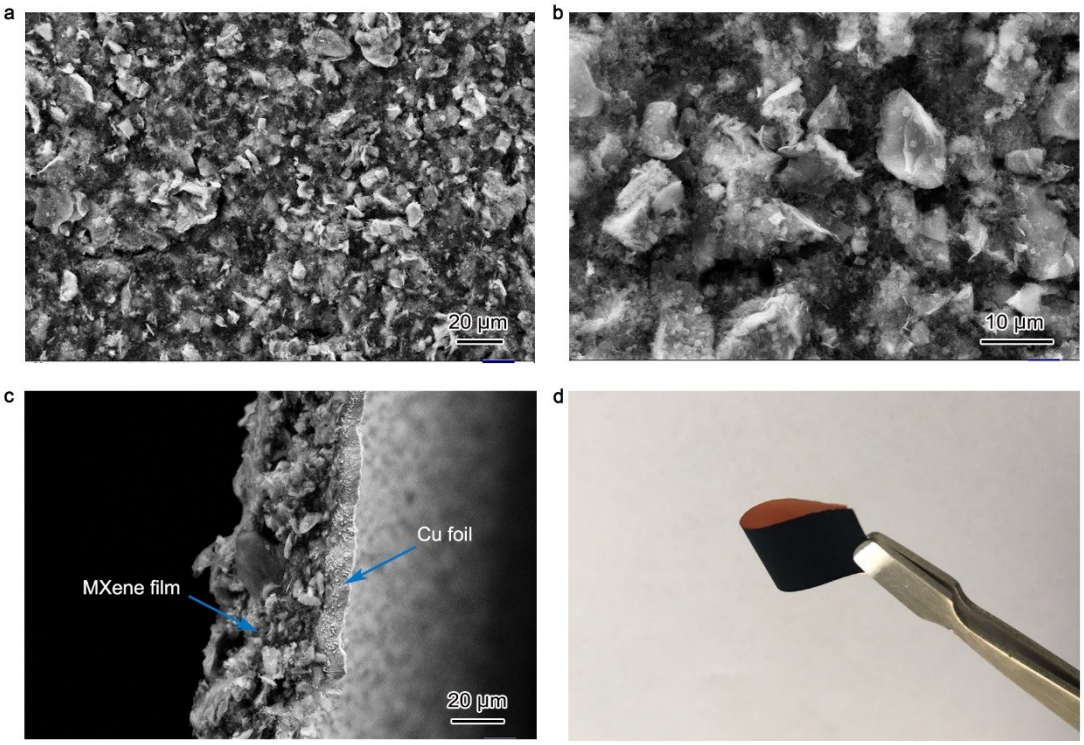

Fig. S2 $Ti_3C_2T_x$ MXene electrode. (a–c) SEM images of $Ti_3C_2T_x$ film coated on Cu foil at (a) low and (b) high magnifications, respectively, and (c) cross sections of the coated film. From the micromorphology of the fabricated electrode, one can see that a well-coated $Ti_3C_2T_x$ film with a thickness of about 20 μm is densely coated on the copper current collector. No defective interface is noticed between the current substrate and the coated $Ti_3C_2T_x$ film, suggesting a good adhesion between them. (d) Flexible $Ti_3C_2T_x$ coated Cu foil electrode, which is readily flexible and easy to be bended arbitrarily.

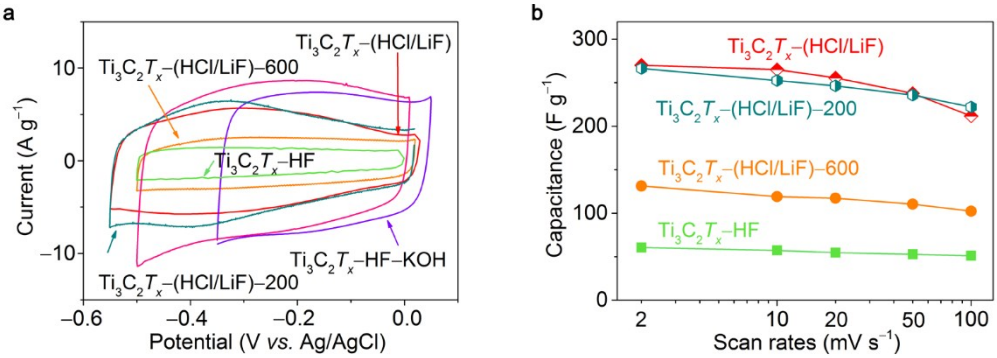

Fig. S3 Capacitive performances of $Ti_3C_2T_x$ electrodes with different preparation methods in 1 mol L^{-1} H_2SO_4 electrolyte. **(**a) CV curves collected at a scan rate of 20 mV s^{-1} and (b) gravimetric capacitances at different scan rates of $Ti_3C_2T_x$ MXenes. $Ti_3C_2T_x$–HF and $Ti_3C_2T_x$–(HCl/LiF) were produced via etching the MAX phase in HF and HCl–LiF solutions, respectively. $Ti_3C_2T_x$–HF–KOH was treated in KOH solution. $Ti_3C_2T_x$–(HCl/LiF)–200, $Ti_3C_2T_x$–(HCl/LiF)–400 and $Ti_3C_2T_x$–(HCl/LiF)–600 was obtained by heating $Ti_3C_2T_x$–(HCl/LiF) in ammonia atmosphere at 200 and 600 °C.

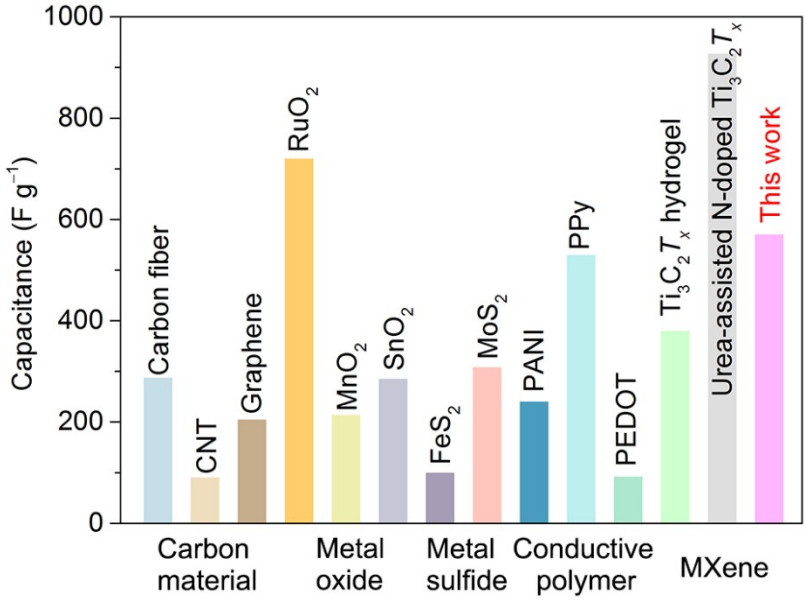

Fig. S4 Capacitance comparison of electrochemical capacitance of various materials.

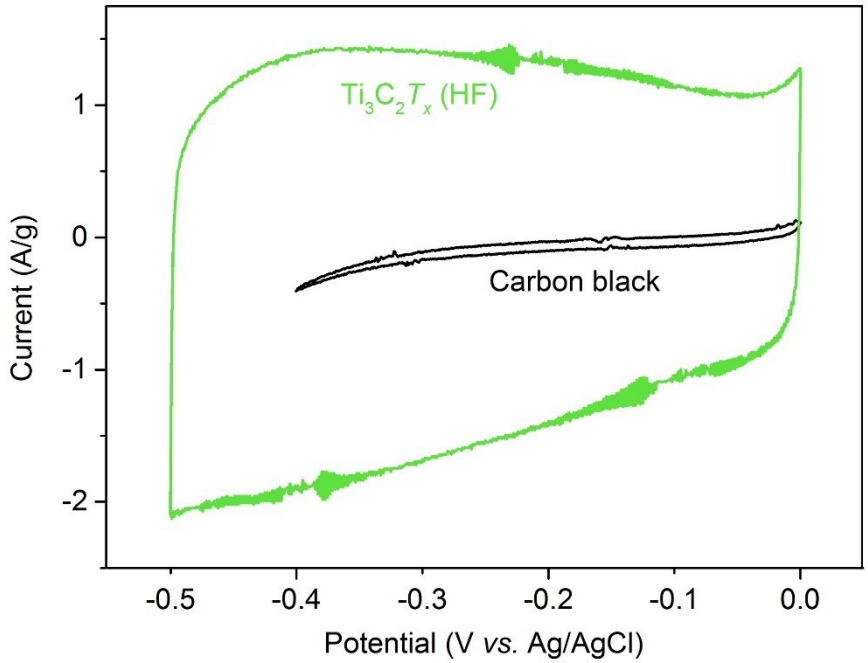

Fig. S5 Electrochemical characterization. CVs of the $Ti_3C_2T_x$–HF electrode and carbon black electrode at scan rate of 20 mV s^{-1} in H_2SO_4 solution, respectively. Note that the carbon black electrode has negligible capacitance. The carbon black electrode was prepared by carbon black and polyvinylidene fluoride in an 8:1 mass ratio dispersed in the N-methyl pyrrolidone to form a slurry, which was then coated onto a copper foil and dried in vacuum at 140 °C for 10 h.

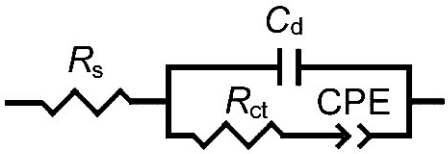

Fig. S6 Equivalent circuit adopted in the simulation of EIS spectra. R_s: electrolyte resistance; C_d: electrical double layer capacitor; R_{ct}: charge transfer resistance; CPE: constant phase angle element.

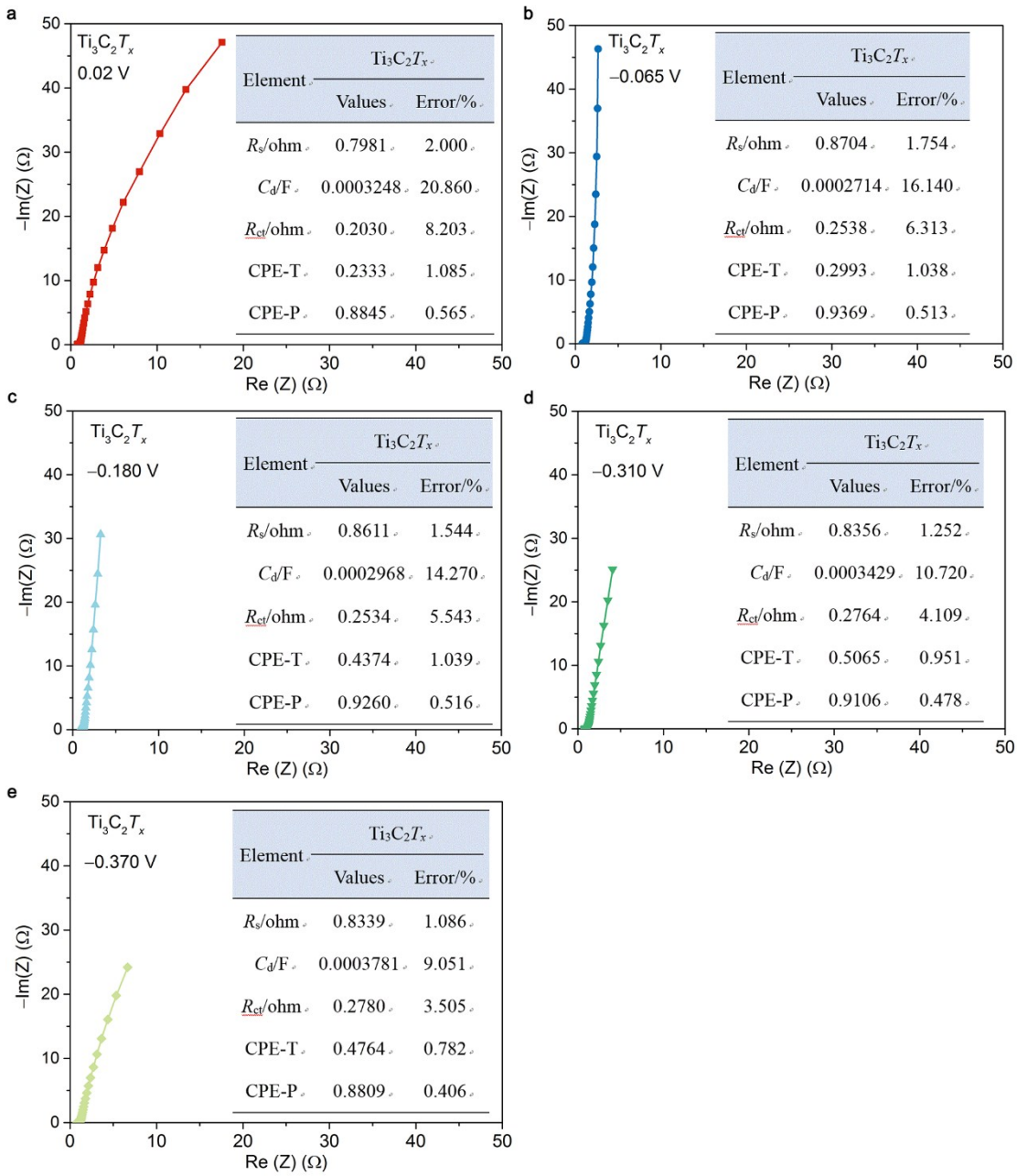

Fig. S7 *In situ* electrochemical EIS spectra. EIS data (Nyquist plots) of $Ti_3C_2T_x$–(HCl/LiF) collected at different potentials *vs.* Ag/AgCl and their corresponding equivalent circuit simulation results.

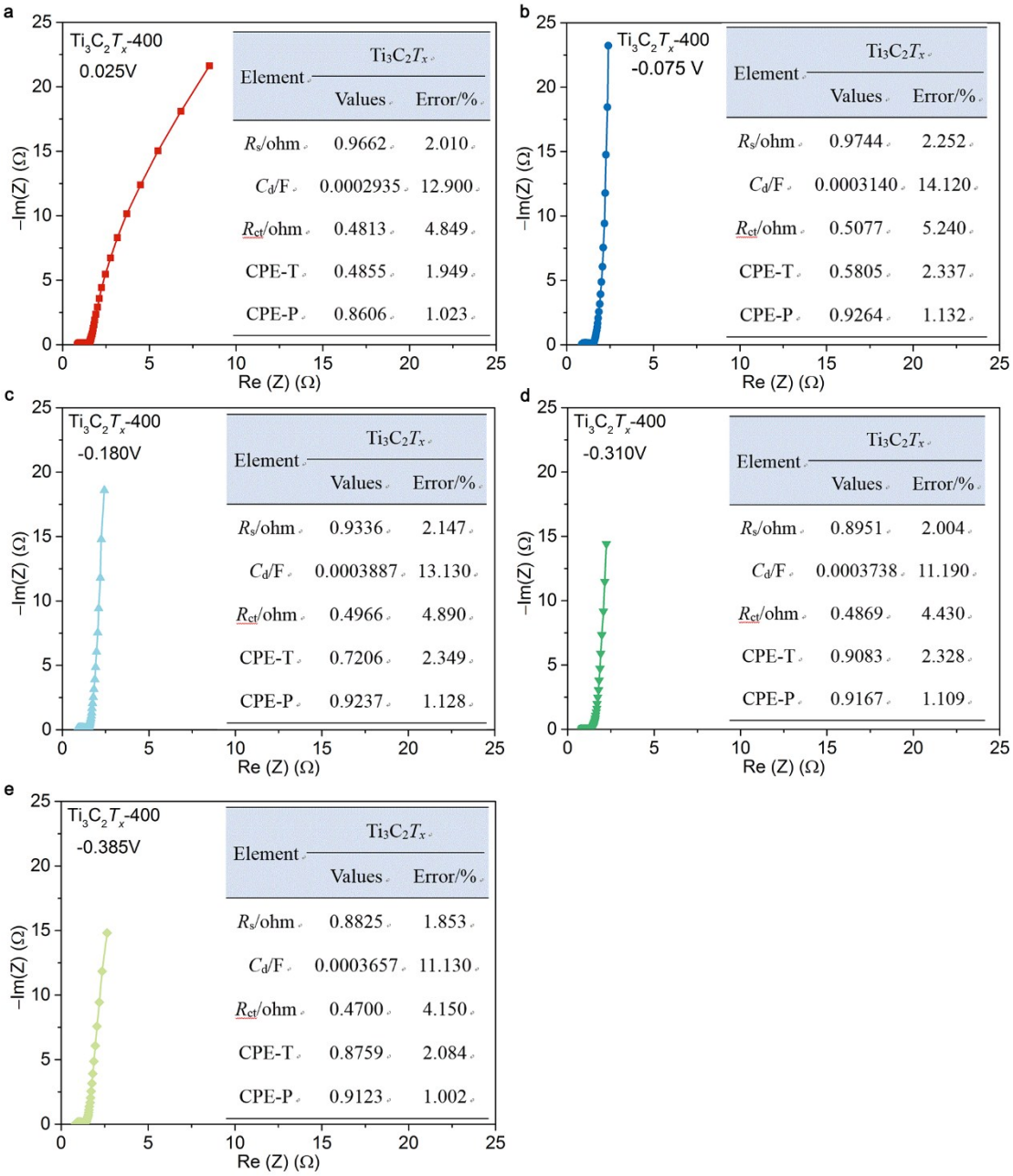

Fig. S8 *In situ* electrochemical EIS spectra. EIS data (Nyquist plots) of $Ti_3C_2T_x$–(HCl/LiF)–400 collected at different potentials *vs.* Ag/AgCl and their corresponding equivalent circuit simulation results.

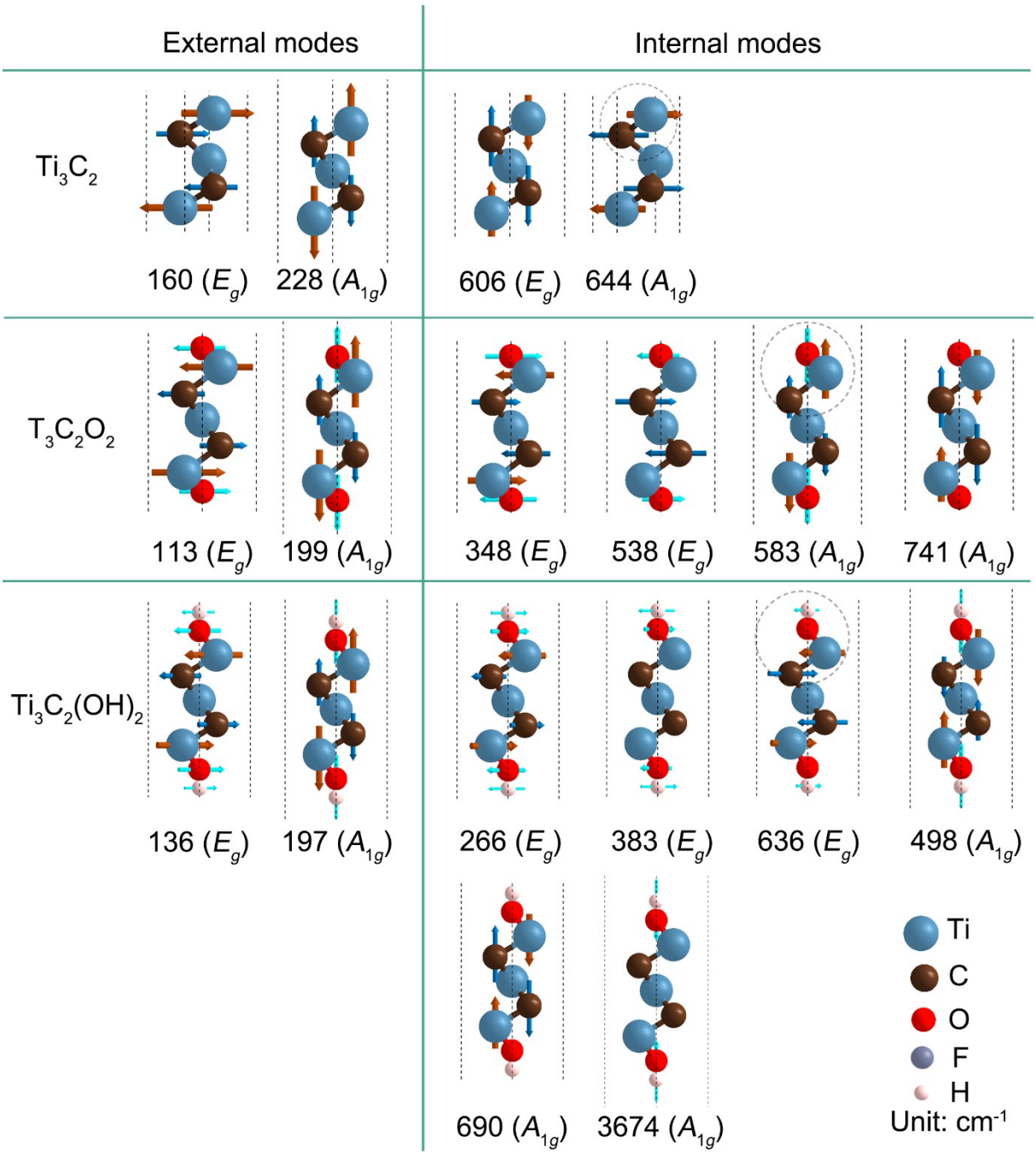

Fig. S9 Schematic of Raman active modes of $Ti_3C_2T_2$ MXene.

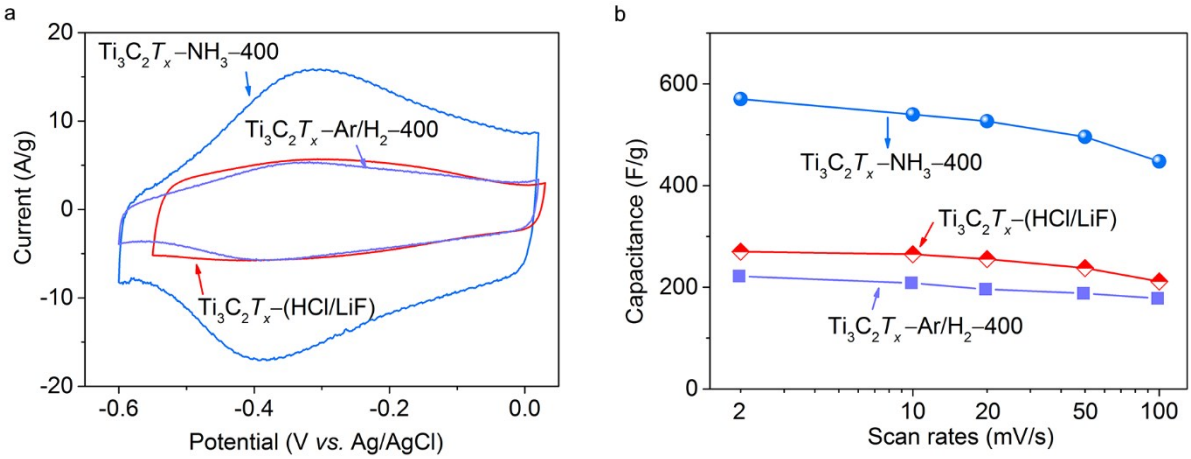

Fig. S10 Capacitive performances of $Ti_3C_2T_x$ electrodes with different preparation methods in 1 mol L^{-1} H_2SO_4 electrolyte. (a) CV curves collected at a scan rate of 20 mV s^{-1} and (b) gravimetric capacitances at different scan rates of $Ti_3C_2T_x$ MXene. $Ti_3C_2T_x$–(HCl/LiF) was produced via etching the MAX phase in HCl–LiF solution. $Ti_3C_2T_x$–NH_3–400 was obtained by heating $Ti_3C_2T_x$–(HCl/LiF) in ammonia atmosphere at 400 °C. $Ti_3C_2T_x$–Ar/H_2–400 was obtained by heating $Ti_3C_2T_x$–(HCl/LiF) in argon/hydrogen atmosphere at 400 °C.

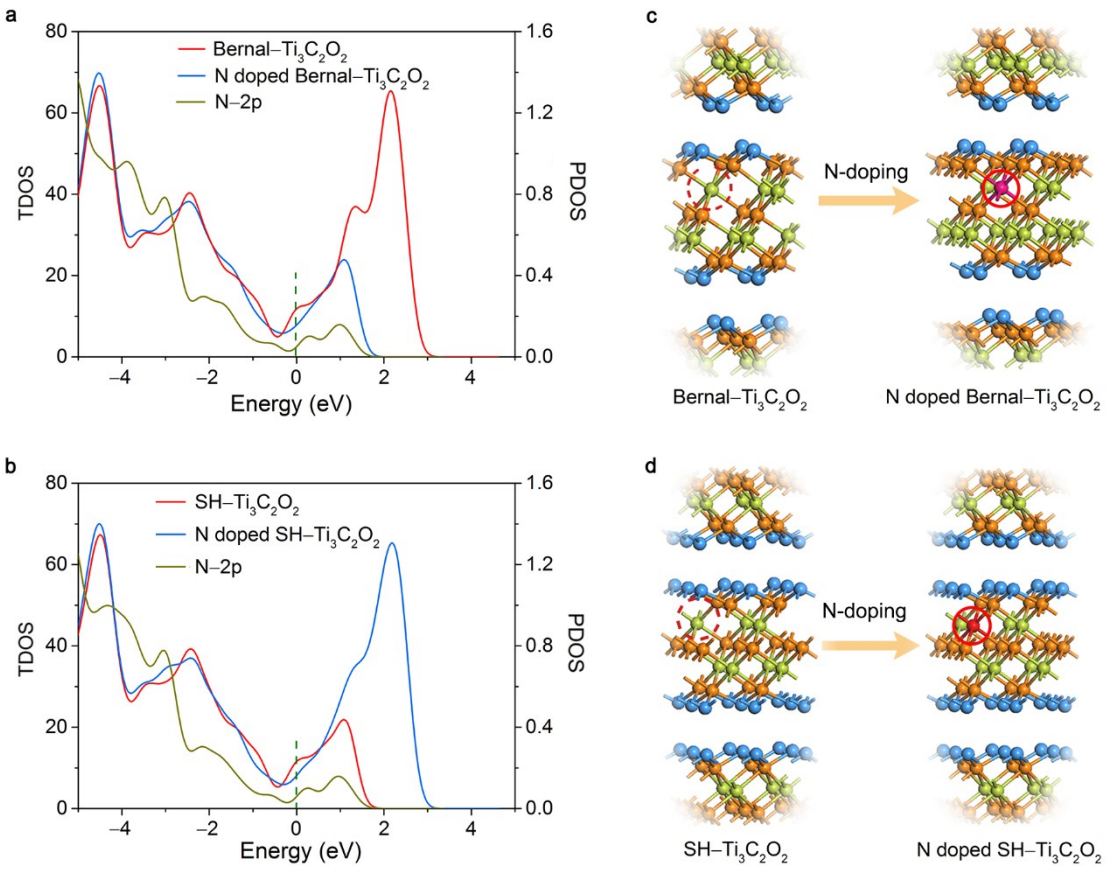

Fig.S11 Density of states. (a,b) Total and partial density of states of multilayer $Ti_3C_2O_2$ with carbon vacancy before and after N doping on the position of carbon vacancy in the two kinds of stacking sequence: (a) Bernal sequence and (b) simple hexagonal (SH) sequence. (c,d) Schematic illustration of their corresponding structure models. Orange color, Ti; light green, C; blue, O; red, N. It is demonstrated that O functional groups terminated $Ti_3C_2T_x$ is most stable in many previous reports,[1,2] so we examined the change of electronic density of states for the N-doped and pristine $Ti_3C_2O_2$ by density functional theory simulation calculations. Since the carbon vacancies are universally present in the MAX phases[3–5], it is believed that their derivatives, MXenes, inherit their hosts' defect. Besides, the layered rather than free-standing MXenes are typically common. So, herein we choose the stacked $Ti_3C_2O_2$ with carbon vacancy as the original $Ti_3C_2O_2$ structure model. After annealing in ammonia, the N atom has an effect on the pristine MXene's structure and Ti-N bond dominates in the N 1s XPS spectra (Fig. 5b), so layered $Ti_3C_2O_2$ with a single N atom substitution at carbon vacancy site is served as the structure model after annealing in ammonia treatment. for multilayer $Ti_3C_2O_2$ with carbon vacancy in both Bernal stacking sequence and SH stacking sequence, a decrease of total density of states in Fermi level is observed after N doping on the position of carbon vacancy, which implied that introducing heteroatomic nitrogen could not increase the conductivity of the MXene.

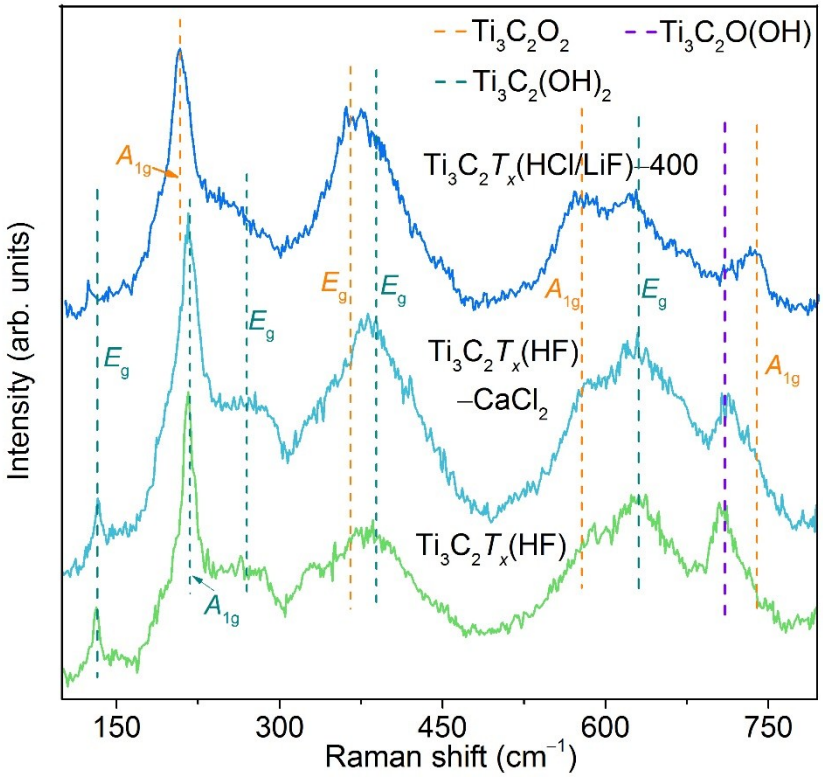

Fig. S12 Raman spectroscopy characterization. Raman spectra of HF etched $Ti_3C_2T_x$ MXene, $CaCl_2$ intercalated HF etched $Ti_3C_2T_x$ MXene and annealing in ammonia (400 °C) treated HCL–LiF etched $Ti_3C_2T_x$ MXene. Dashed lines represent the simulated Raman active vibrational mode peaks of the $Ti_3C_2T_x$ terminated different functional groups.

Table S1 Atomic percent in $Ti_3C_2T_x$–(HCl/LiF)–400 and $Ti_3C_2T_x$–HF–KOH obtained by XPS analysis.

Atomic percent (%)	Ti 2p	C 1s	Al 2p	O 1s	F 1s	Cl 2p	N 1s	K2p
$Ti_3C_2T_x$–(HCl/LiF)–400	27.7	32.9	3.4	22.6	9.5	1.2	2.7	--
$Ti_3C_2T_x$–HF–KOH	28.9	30.8	0	26.7	9.6	1.9	1.1	1.0

In one $Ti_3C_2T_x$ unit, there are three 3 Ti atoms. Therefore, according to the atomic percent, there are 2.45 O atoms in one $Ti_3C_2T_x$ unit for $Ti_3C_2T_x$–(HCl/LiF)–400 while 2.77 O atoms for $Ti_3C_2T_x$–HF–KOH. Based on the percentage of various moieties in O 1s spectra, we can deduce that the following formulae:

$Ti_3C_2T_x$–(HCl/LiF)–400 $Ti_3C_2(OH)_{0.66}O_{1.60}(ON)_{0.2}$

$Ti_3C_2T_x$–HF–KOH $Ti_3C_2(OH)_{1.22}O_{1.55}$

References

1 T. Hu, Z. Li, M. Hu, J. Wang, Q. Hu, Q. Li and X. Wang, *J. Phys. Chem. C*, 2017, **121**, 19254.

2 J. Halim, K. M. Cook, M. Naguib, P. Eklund, Y. Gogotsi, J. Rosen and M. W. Barsoum, *Appl. Surf. Sci.*, 2015, **362**, 406.

3 J. Etzkorn, M. Ade and H. Hillebrecht, *Inorg. Chem.*, 2007, **46**, 7646.

4 H. Zhang, T. Hu, X. Wang, Z. Li, M. Hu, E. Wu and Y. Zhou, *Sci. Rep.*, 2015, **5**, 14192.

5 H. Zhang, T. Hu, Z. Li, Y. Zhang, M. Hu, X. Wang and Y. Zhou, *J. Am. Ceram. Soc.*, 2017, **100**, 724.